

Gemini Surfactants at Solid–Liquid Interfaces: Control of Interfacial Aggregate Geometry

S. Manne,^{*,†} T. E. Schäffer,[‡] Q. Huo,[§] P. K. Hansma,[‡] D. E. Morse,^{||}
G. D. Stucky,[§] and I. A. Aksay[†]

Princeton Materials Institute and Department of Chemical Engineering, Princeton University, Princeton, New Jersey 08544-5263, and Departments of Physics, Chemistry, and Molecular, Cellular and Developmental Biology, University of California, Santa Barbara, California 93106

Received January 22, 1997. In Final Form: June 2, 1997[®]

Recent work has shown that conventional surfactants form ordered aggregates of well-defined shape and size at solid–liquid interfaces.^{1,2} Here we report interfacial aggregate structures as a function of surfactant geometry by using gemini surfactants with varying tail and spacer lengths. On the anionic cleavage plane of mica, aggregates tend to favor a lower curvature than in solution but follow the same general variation with surfactant geometry (i.e., with larger headgroup areas resulting in greater curvature). These morphologies on mica correlate well with those observed in surfactant–silicate mesophases, where electrostatic binding of headgroups also plays a dominant role. In addition, interfacial sphere-to-rod transitions are induced on mica (as in free solution) by binding with a headgroup-specific counterion. In contrast to mica, the hydrophobic cleavage plane of graphite interacts with surfactant tailgroups, giving rise to interfacial aggregates that are surface-controlled and relatively independent of surfactant geometry. This interaction is used to heterogeneously nucleate a surfactant–silicate mesophase which is interfacially controlled and differs from the bulk phase.

Introduction

The modification of surfactant self-assembly due to interaction with foreign moieties is a phenomenon common to both solution-phase applications and interfacial adsorption and aggregation. In particular, the synthesis of mesoscopic silicates by surfactant-based templating^{3–7} involves a complex set of interactions between surfactant aggregates, multivalent counterions, and solvent molecules in a process which is not completely understood. For heterogeneous nucleation of mesoscopic films at solid–liquid interfaces,^{8–10} an additional complication is the effect of the interface, which can be either hydrophilic or hydrophobic. No predictive models exist as yet for interfacial surfactant phases as a function of molecular geometry and surface chemistry, and the effect of silicates on interfacial phases is unknown, especially in cases where the constraints of the interface may conflict with the surfactant–silicate phase favored in solution. Knowledge of interfacial aggregation, therefore, not only complements our understanding of solution-phase micellization but also has relevance for device applications involving surfactant-templated thin films and membranes (complementing

existing strategies involving, e.g., covalent self-assembly¹¹ and Langmuir–Blodgett films¹²). Here we investigate the variables involved in regulating interfacial surfactant morphology, with the eventual goal of designing novel mesoscopic thin films and membranes that are chemically accessible from a variety of orientations.

Gemini or dimeric surfactants¹³ have been generating increasing interest owing to their superior performance in applications and their tunable molecular geometry. Geminis consist of two conventional single-tail surfactants whose headgroups are joined covalently by a spacer (usually hydrophobic) of variable length. In aqueous solutions, geminis spontaneously aggregate into micelles whose shape and size are highly sensitive to the length of this hydrophobic spacer. Geminis are therefore important for fundamental studies of self-assembly, since they offer a way to modify the “dimensionless packing parameter” g in a well-defined and nearly continuous fashion.¹⁴ Most such investigations have focused (as we do here) on geminis with linear hydrocarbon tailgroups and quaternary ammonium headgroups,^{15–20} given by the general formula $(C_n H_{2n+1}) [N^+(CH_3)_2](CH_2)_s [N^+(CH_3)_2]$

* Author to whom correspondence should be addressed. Permanent address: Department of Physics, University of Arizona, Tucson, Arizona 85721, USA.

† Princeton Materials Institute and Department of Chemical Engineering, Princeton University.

‡ Department of Physics, University of California.

§ Department of Chemistry, University of California.

|| Department of Molecular, Cellular, and Developmental Biology, University of California.

® Abstract published in *Advance ACS Abstracts*, October 15, 1997.

(1) Manne, S.; Cleveland, J. P.; Gaub, H. E.; Stucky, G. D.; Hansma, P. K. *Langmuir* **1994**, *10*, 4409–4413.

(2) Manne, S.; Gaub, H. E. *Science* **1995**, *270*, 1480–1482.

(3) Beck, J. S.; et al. *J. Am. Chem. Soc.* **1992**, *114*, 10834–10843.

(4) Monnier, A.; et al. *Science* **1993**, *261*, 1299–1303.

(5) Huo, Q.; et al. *Chem. Mater.* **1994**, *6*, 1176–1191.

(6) Firouzi, A.; et al. *Science* **1995**, *267*, 1138–1143.

(7) Huo, Q.; Leon, R.; Petroff, P. M.; Stucky, G. D. *Science* **1995**, *268*, 1324–1327.

(8) Yang, H.; Kuperman, A.; Coombs, N.; Mamiche-Afara, S.; Ozin, G. A. *Nature* **1996**, *379*, 703–705.

(9) Mann, S.; Ozin, G. A. *Nature* **1996**, *382*, 313–319.

(10) Aksay, I. A. et al. *Science* **1996**, *273*, 892–898.

(11) Kumar, A.; Biebuyck, H. A.; Whitesides, G. M. *Langmuir* **1994**, *10*, 1498–1516.

(12) Ulman, A. *An Introduction to Ultrathin Organic Films: From Langmuir–Blodgett to Self-Assembly*; Academic Press: Boston, MA, 1991.

(13) For reviews see: (a) Zana, R. *Curr. Opin. Colloid Interface Sci.* **1996**, *1*, 566–571. (b) Rosen, M. J. *CHEMTECH* **1993**, 30–33.

(14) This parameter reflects the effective molecular geometry of a given surfactant molecule in a micelle and is defined as $g = v/(al)$, where v is the hydrocarbon chain volume, a is the optimum headgroup area per molecule, and l is the hydrocarbon chain length. Spherical micelles are favored when $g < 1/3$, cylinders are favored when $1/3 < g < 1/2$, and bilayers and vesicles are favored when $1/2 < g < 1$. See: Israelachvili, J. N.; Mitchell, D. J.; Ninham, B. W. *J. Chem. Soc., Faraday Trans. 1* **1976**, *72*, 1525–1568.

(15) Zana, R.; Benraou, M.; Rueff, R. *Langmuir* **1991**, *7*, 1072–1075.

(16) Alami, E.; Levy, H.; Zana, R.; Skoulios, A. *Langmuir* **1993**, *9*, 940–944.

(17) Hagslåt, H.; Söderman, O.; Jönsson, B. *Langmuir* **1994**, *10*, 2177–2187.

(18) Danino, D.; Talmon, Y.; Zana, R. *Langmuir* **1995**, *11*, 1448–1456.

(19) Karaborni, S.; et al. *Science* **1994**, *266*, 254–256.

(C_mH_{2m+1}) $\cdot 2Br^-$, hereafter C_{n-s-m} for short, where n and m are the number of carbon atoms in the two tails and s is the number of carbon atoms in the spacer. Previous studies¹⁸ have shown that for micelles of symmetric geminis ($n = m$), the effective headgroup area increases with increasing s (up to $s = 7$ or so), owing to the repulsion between the two positive charge centers which stretches out the spacer between them. Thus the effective molecular geometry is wedgelike ($1/3 < g < 1/2$) for molecules with small spacers ($s = 2$ or 3), resulting in cylindrical micelles, whereas the geometry is conelike ($g < 1/3$) for larger spacers, resulting in spherical or spheroidal micelles. On the other hand, highly asymmetric geminis—specifically the extreme case $m = 1$ —act like conventional surfactants with highly repulsive headgroups,¹⁷ giving rise to large headgroup separations and spherical micelles ($g < 1/3$).

While the free aggregation properties of gemini surfactants have been extensively studied,^{15–19} aggregation at interfaces has received little attention so far.²⁰ Recent work^{1,2,21} using atomic force microscopy (AFM)²² has shown that interfacial aggregates of conventional surfactants can differ markedly from those in free solution. Here we report the aggregation properties of symmetric and asymmetric gemini surfactants at model hydrophilic and hydrophobic surfaces (mica and graphite, respectively) in aqueous solutions. Our aim was to investigate two-dimensional aggregate morphologies in the wide concentration regime where the surface is effectively saturated with surfactant but three-dimensional mesophases are absent. Adsorption isotherms typically show a wide plateau (discussed below) from the critical micelle concentration (cmc) to the onset of the first liquid crystalline mesophase, indicating little change in the interfacial self-assembly morphology in this concentration regime. Accordingly, we used solution concentrations in this “dilute micellar” regime, typically one to two times the cmc; occasional experiments at concentrations up to ~ 100 times the cmc showed no qualitative differences in interfacial self-assembly.

AFM results show that aggregates at the negatively charged mica interface have lower curvature and/or greater degree of ordering than those in the surrounding solution, in close analogy with the spontaneous ordering of micelles found in surfactant–silicate mesophases. Nevertheless, aggregate shape vs packing parameter on mica follows the same general trend as in free solution, with larger g values corresponding to lower curvature. In contrast, aggregates at the hydrophobic graphite interface are observed to be surface-directed and relatively independent of g . This difference in the degree of surface control is highlighted by two contrasting results: the induction of a sphere-to-rod transition on mica by a specifically binding counterion and the heterogeneous nucleation of a surfactant–silicate mesophase on graphite which is interfacially controlled and differs from the bulk phase.

Experimental Section

We chose gemini surfactants that form micelles at room temperature, have known phase behavior in free solution,^{15–19} and span a wide range of molecular geometries. The surfactants used herein are divided into three categories based on their known phase behavior in solution (Table 1, column 1): (i) fully asymmetric geminis ($m = 1$, $s = 3$, $n = 12$, 16, and 18); (ii) symmetric geminis with moderate spacer length ($m = n = 12$,

$s = 4$ and 6); (iii) symmetric gemini with a short spacer ($m = n = 12$, $s = 2$). These surfactants were synthesized and purified as described previously.¹⁵ Surfactants in each category also gave rise to similar interfacial aggregates, so only representative images in each category are shown below. Mica and graphite crystals were cleaved just prior to use.

Interfacial aggregates were imaged directly by AFM using precontact repulsive forces, as described previously.¹ Briefly, this method involves imaging with colloidal stabilization forces (electric double layer and other short-range forces) established between the tip and sample, arising from surfactant adsorption on the two surfaces. We used a commercial AFM (Nanoscope III from Digital Instruments, Santa Barbara, CA) and commercial silicon (Park Scientific Instruments, Sunnyvale, CA) or silicon nitride (Digital Instruments) cantilevers cleaned by exposure to ultraviolet light (15–60 min). Typical imaging forces were 0.1–1 nN and imaging times 30–90 s. Scan frequencies used were from ~ 5 to 15 Hz and had little effect on the data observed. Experiments were performed at room temperature in Millipore water. All images shown are unfiltered except for slope removal along scan lines. Images were calibrated by pushing through the surfactant layer at high force and imaging the underlying lattice, which also permitted a comparison of relative orientations.

Results and Discussion

The cleavage plane of mica is negatively charged and interacts electrostatically with the headgroups of cationic surfactants. Aggregate morphologies of gemini surfactants at the mica–solution interface were observed to vary with surfactant geometry (Figure 1). The asymmetric gemini surfactants C_{n-3-1} (smallest g) formed globular aggregates arranged in a hexagonal pattern (Figure 1A). This “aggregate lattice” had a nearest-neighbor spacing of ~ 50 – 80% over the expected micelle diameter, taken to be twice the surfactant length (see below), and its symmetry axes were aligned with the underlying mica symmetry axes on average, although sometimes exhibiting dislocations (lower half of Figure 1A). The symmetric gemini surfactants $C_{12-4-12}$ and $C_{12-6-12}$ (intermediate g) formed parallel linear aggregates or stripes (Figure 1B) similar to those of conventional alkyltrimethylammonium surfactants. The measured stripe spacing (4.3 ± 0.4 nm) was a little over twice the length of a dodecane tailgroup, and cylinders of $C_{12-4-12}$ (and to a lesser extent $C_{12-6-12}$) were on average oriented parallel to the mica symmetry axes. Finally, the gemini with a short spacer $C_{12-2-12}$ (largest g) gave rise to featureless images (Figure 1C) indicative of a planar aggregate.

The aggregate morphologies of parts A–C of Figure 1 are interpreted respectively as hexagonally packed spheres (C_{n-3-1}), parallel cylinders ($C_{12-4-12}$ and $C_{12-6-12}$), and a flat bilayer ($C_{12-2-12}$), with the spherical and cylindrical aggregates probably flattened on the bottom to conform to the mica plane. These identifications are based on comparison with known adsorption characteristics of conventional quaternary ammonium surfactants, whose headgroups and tailgroups are chemically identical to those of the geminis. Surface force apparatus (SFA) measurements^{23,24} have indicated adsorbed layer thicknesses of between one and two surfactant lengths for quaternary ammonium surfactants on mica (from micellar solutions). Similar thicknesses have been measured by neutron reflectivity^{25,26} on anionic silica surfaces, and recent work²⁶ has additionally confirmed that headgroups

(23) Pashley, R. M.; Israelachvili, J. N. *Colloids Surf.* **1981**, *2*, 169–187.

(24) Kekicheff, P.; Christenson, H. K.; Ninham, B. W. *Colloids Surf.* **1989**, *40*, 31–41.

(25) McDermott, D. C.; McCarney, J.; Thomas, R. K.; Rennie, A. R. *J. Colloid Interface Sci.* **1994**, *162*, 304–310.

(26) Fragneto, G.; Thomas, R. K.; Rennie, A. R.; Penfold, J. *Langmuir* **1996**, *12*, 6036–6043.

(20) Alami, E.; Beinert, G.; Marie, P.; Zana, R. *Langmuir* **1993**, *9*, 1465–1467.

(21) Wanless, E. J.; Ducker, W. A. *J. Phys. Chem.* **1996**, *100*, 3207–3214.

(22) Binnig, G.; Quate, C. F.; Gerber, Ch. *Phys. Rev. Lett.* **1986**, *56*, 930–933.

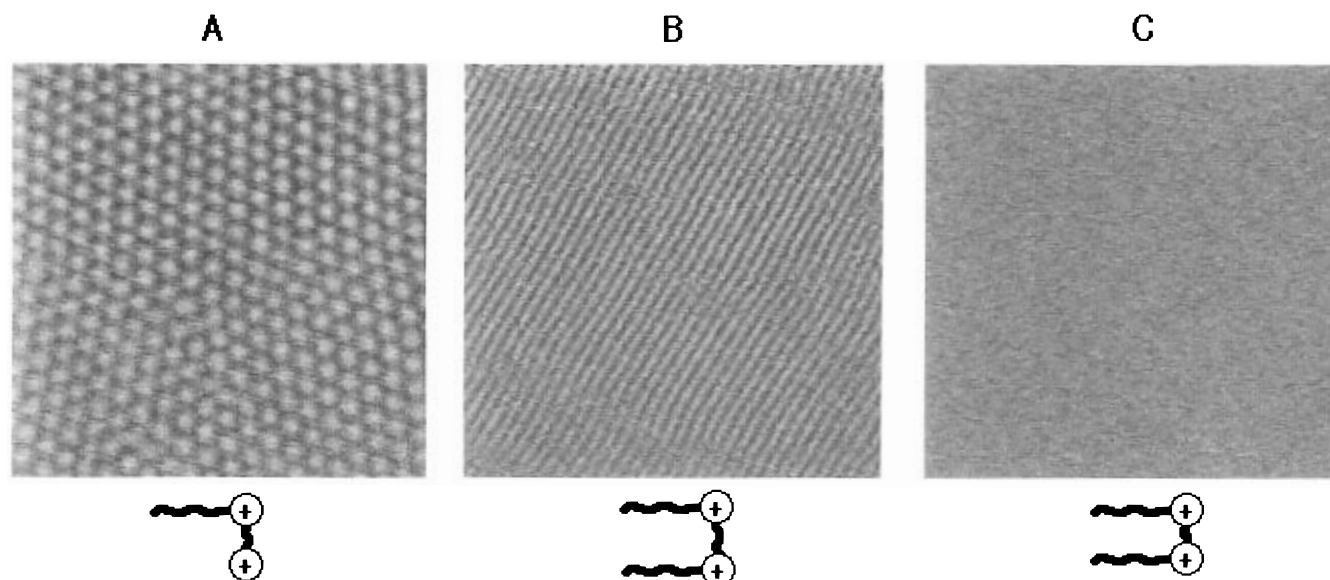







Figure 1. AFM images (150×150 nm) of gemini surfactant aggregates on the cleavage plane of mica in contact with aqueous surfactant solution. (A) Asymmetric gemini surfactant C_{18-3-1} (3.0 mM solution), showing spherical aggregates in a hexagonal lattice with a nearest-neighbor distance of 8.8 ± 0.7 nm. Other asymmetric geminis also showed spherical aggregates, with nearest-neighbor distances roughly proportional to surfactant chain length (7.0 ± 0.7 nm for C_{16-3-1} and 5.1 ± 0.4 nm for C_{12-3-1}). (B) Symmetric gemini surfactant $C_{12-4-12}$ (2.2 mM solution, or $2 \times \text{cmc}^{15}$), showing cylindrical aggregates oriented along a mica symmetry axis, with a spacing of 4.2 ± 0.4 nm. $C_{12-6-12}$ also showed cylindrical aggregates at similar spacings. (C) Symmetric gemini surfactant $C_{12-2-12}$ (1.0 mM solution, or $1.3 \times \text{cmc}^{15}$); images are featureless, indicating a flat bilayer.

Table 1. Aggregate Morphologies for Conventional and Gemini Surfactants in Free Aqueous Solution (column 1), in Surfactant–Silicate Mesophases (column 2), at the Mica–Solution Interface (column 3), and at the Graphite–Solution Interface (Column 4)^a

cationic surfactant	micelle shape (micelle packing symmetry)			
	in pure solution	in silicate mesophase	at mica surface	at graphite surface
 asymmetric gemini (e.g., C_{18-3-1}), $g < 1/3$	spheres (isotropic)	spheres (3-dimensional hexagonal)	spheres (2-dimensional hexagonal)	half-cylinders (parallel)
 conventional alkyl-trimethylammonium, $g \approx 0.33$	spheres (isotropic)	cylinders (hexagonal)	cylinders (parallel)	half-cylinders (parallel)
 symmetric gemini $s \geq 4$ (e.g., $C_{12-4-12}$), $g \approx 0.33$	spheres & spheroids (isotropic)	cylinders (hexagonal)	cylinders (parallel)	half-cylinders (parallel)
 symmetric gemini, $s = 2$ ($C_{12-2-12}$), $1/3 < g < 1/2$	cylinders (isotropic)	bilayers (lamellar)	bilayer	half-cylinders (parallel)
 conventional dialkyl-dimethylammonium, $g \approx 0.62$	bilayers & vesicles (isotropic)	bilayers (lamellar)	bilayer	

^a Surfactants are arranged in order of increasing dimensionless packing parameter g .^{17,18,37} All aggregate morphologies correspond to the dilute micellar concentration regime (i.e., far below the onset of lyotropic liquid-crystalline phases in solution). Both the aggregate shape and the symmetry of aggregate arrangement are indicated. Data in the first column are from refs 17, 18, and 37. Data in the second column are from refs 3, 5, and 7. Data in the third and fourth columns are from this work and from refs 1 and 2.

occupy both the inside and outside of the interfacial aggregates. (It is worth noting that adsorbate thickness cannot be accurately determined by precontact AFM images, since the AFM effectively plots an equipotential surface at some separation above the adsorbate layer.) These results provide strong evidence that the interfacial self-assembly is dominated by headgroup–surface electrostatic interactions, resulting in flattened but full-micellar aggregates²⁶ (i.e., with only headgroups exposed to the solution and surface). They additionally preclude the existence of aggregate multilayers, which are in any case not expected for surfactant concentrations far below the first mesophase boundary. (Whereas the first aggregate layer is electrostatically attracted to the surface, multilayer formation must overcome an electrostatic repulsion to the first layer.) This is further corroborated by recent adsorption measurements for $C_{12-2-12}$ on silica²⁷

showing that surface saturation is reached with an adsorbed bilayer above the cmc.

The gemini aggregate morphologies on mica are summarized in Table 1 (column 3), along with earlier results on conventional surfactants, arranged in order of increasing g . The dimensionless packing parameter is seen to play a similar role in interfacial aggregation on mica as it does in bulk aggregation; as g increases, aggregate shapes change from spheres (high curvature) to cylinders (intermediate curvature) to bilayers (low curvature). However, aggregates on mica favor a curvature lower than (or equal to) the corresponding free aggregates. We propose that this arises from the electrostatic binding of headgroups; i.e., the mica surface acts as a highly charged,

(27) Esumi, K.; Goino, M.; Koide, Y. *Colloids Surf.* **1996**, *118*, 161–166.

laterally extended "counterion", which allows a closer packing of headgroups at the surface than is found in free micelles. The resulting small increase in g at the interface causes a transition to lower aggregate curvature for surfactants with borderline g values (e.g., alkyltrimethylammonium surfactants) but not for surfactants whose g is far from a transitional value (e.g., asymmetric gemini surfactants). For example, the cylindrical interfacial aggregation of $C_{12-4-12}$ (which forms spherical micelles in solution) can be regarded as a surface-induced sphere-to-rod transformation, in the same way that excess counterions induce similar transformations in solution.²⁸

Aggregates on mica are also fairly ordered and are spaced much closer together than in solution, resembling a concentrated bulk phase but in two dimensions. Such creation of lyotropic liquid-crystalline phases at dilute surfactant concentrations is also a hallmark of mesoporous silicate synthesis using surfactant micelles.⁵ (In this process,³ mesoporous silicate frameworks are synthesized by mixing soluble silicate anions with cationic surfactants in aqueous solution, isolating the resulting surfactant-silicate composite material, and removing the surfactant by pyrolysis.) Even in dilute solutions, the strong electrostatic interaction between the cationic headgroups and the silicate counterions causes both lower aggregate curvature and clustering of aggregates into lyotropic phases.⁵ It is instructive to compare the observed interfacial aggregate morphologies on mica with published surfactant-silicate mesophases in bulk solution (Table 1, columns 2 and 3). In each case the former is a two-dimensional form of the latter, suggesting that similar headgroup binding mechanisms operate in the two systems. In the surfactant-silicate system, charge density matching between aggregate surfaces and multivalent silicate counterions drives mesophase formation in three dimensions,^{5,6} whereas in the surfactant-mica system, charge density matching between aggregate surfaces and the mica plane controls interfacial self-assembly in two dimensions.

The binding geometry is of course significantly different in the two systems; charge neutralization by silicates occurs symmetrically over the micelle surface, whereas charge neutralization by the mica plane occurs only on the bottom surface of the micelle. (Aggregates on mica are probably asymmetric as a result, the bottom surface being flattened to conform to the mica plane; AFM images cannot resolve this detail.) Thus the electrostatic repulsion between neighboring aggregates (especially spheres) should be greater on the mica surface than in a silicate mesophase. This may account for the larger interaggregate spacing found for spheres of C_{n-3-1} on mica. Normalizing to the tail length l using Tanford's formula,²⁹ the nearest-neighbor distance for spheres on mica varied from $3.1l$ to $3.6l$, as compared to $2.7l$ for C_{n-3-1} -silicate mesophases.⁷ It is also interesting to note that cylindrical aggregates on mica (and half-cylindrical ones on graphite, see below) had smaller spacings ($2.4l$ to $2.8l$) than spherical aggregates, consistent with the greater degree of charge neutralization expected for cylindrical curvature.

Recently a surface-aggregate shape transformation on mica has been reported, resulting from competitive adsorption in a mixture of a cationic and a zwitterionic surfactant.³⁰ Both surfactants adsorb to mica, with the pure cationic surfactant forming cylindrical aggregates and the pure zwitterionic forming spherical aggregates

above the cmc; the shape transformation results from the gradual displacement of one surfactant species by the other over a period of hours. Interfacial patterns formed by micelles can also in principle be modified by effecting a micellar shape transition, e.g., a sphere-to-rod transition, by *direct binding to the aggregates themselves* (not to the mica surface). Unlike the free solution case,²⁸ however, spherical aggregates on mica were observed to be fairly insensitive to counterion concentration; the spherical morphology of C_{n-3-1} remained insensitive to Br^- concentrations up to 1.5 M and even to moderate concentrations of multivalent counterions such as SO_4^{2-} and citrate³⁻ (although the image quality became steadily worse). This insensitivity is perhaps understandable given that the mica surface *already* acts as a highly charged counterion, which nevertheless fails to induce a sphere-to-rod transition in C_{n-3-1} surfactants. Only a surfactant-specific counterion with a known high affinity for quaternary ammonium headgroups, namely salicylate,³¹ proved successful. Exposure of C_{n-3-1} solutions to small amounts of sodium salicylate caused a transformation of the interfacial pattern from hexagonally packed dots to parallel but flexible lines (Figure 2). This transformation was accompanied by a reduction in interaggregate spacing (from 8.8 to 6.2 nm), consistent with a greater degree of charge neutralization for the cylinders due to salicylate binding. This transformation was also reversible, giving rise to hexagonally packed spheres again upon exchange with pure surfactant solution. One advantage of this sphere-to-rod transformation based on direct aggregate binding is that the equilibration time (<2 min) is much faster, since it does not rely on slow surface exchange of adsorbed molecules.³⁰

While interfacial phases on mica showed some dependence on surfactant geometry, interfacial phases on the hydrophobic cleavage plane of graphite were observed to be surface-directed and virtually independent of g . Interfacial aggregates of gemini surfactants were predominantly in the form of parallel stripes (Figure 3) oriented *perpendicular* to an underlying symmetry axis of graphite, exactly as observed with conventional quaternary ammonium surfactants.^{1,2} For these the stripes have been identified previously^{1,2} as half-cylinders (with the bottom row of tailgroups oriented parallel to a graphite symmetry axis), by relating the AFM images to (i) molecular occupational areas known from adsorption isotherms^{32,33} and (ii) preferred orientation of alkyl derivatives parallel to substrate symmetry axes.³⁴ Observation of the identical aggregate shapes and orientations with gemini surfactants suggests that these aggregates are also half-cylindrical, driven by strong tailgroup-surface interactions. Maximizing the dispersion and hydrophobic interactions in this way constrains the aggregate morphology. The surface lattice thus controls the aggregation process, with surfactant geometry evidently playing a relatively minor role.

Although half-cylindrical aggregates on graphite are not too surprising for surfactants with intermediate g

(31) Salicylate and other phenyl derivatives are known to induce sphere-to-rod transitions in free solutions of quaternary ammonium surfactants, by reducing the headgroup area due to strong binding and charge neutralization. This high binding strength arises from the partially hydrophobic character of these counterions, which results in a combination of electrostatic interactions with headgroups and hydrophobic interactions with the adjacent carbon atoms in the tailgroup. See Cassidy, M. A.; Warr, G. G. *J. Phys. Chem.* **1996**, *100*, 3237-3240 and references therein.

(32) Saleeb, F. Z.; Kitchener, J. A. *J. Chem. Soc.* **1965**, 911-917.

(33) See: Zettlemoyer, A. C. *J. Colloid Interface Sci.* **1968**, *28*, 343-369 and the discussion in ref. 1.

(34) (a) Groszek, A. *J. Proc. R. Soc. London, Sect. A* **1970**, *314*, 473-498. (b) Rabe, J. P.; Buchholz, S. *Science* **1991**, *253*, 424-427. (c) Yeo, Y. H.; Yacoboski, K.; McGonigal, G. C.; Thompson, D. J. *J. Vac. Sci. Technol., A* **1992**, *10*, 600-602.

(28) See for example Quirion, F.; Magid, L. J. *J. Phys. Chem.* **1986**, *90*, 5435-5441.

(29) Tanford, C. *The Hydrophobic Effect*; John Wiley & Sons: New York, 1973.

(30) Ducker, W. A.; Wanless, E. J. *Langmuir* **1996**, *12*, 5915-5920.

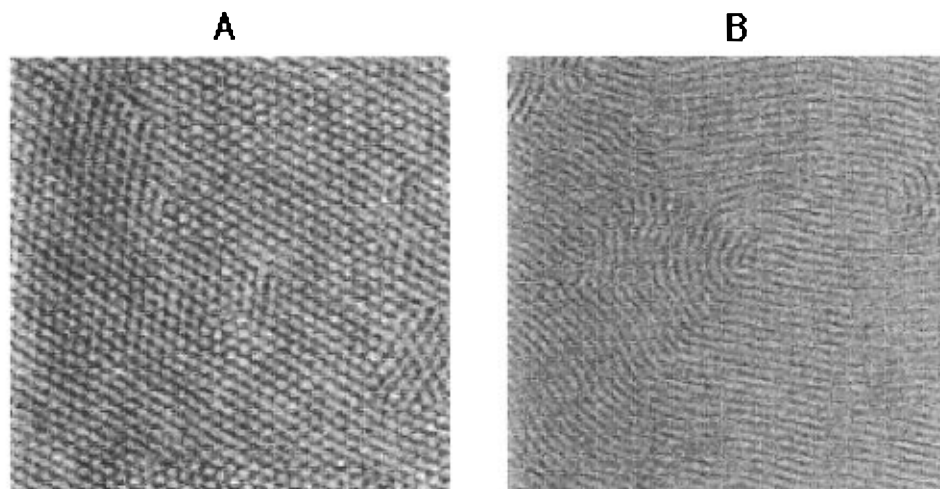


Figure 2. AFM images of the same sample area (280×280 nm) showing surface aggregates of C_{18-3-1} on mica (A) before and (B) 10 min after placing a drop of sodium salicylate solution in contact with C_{18-3-1} solution in the AFM fluid cell. (The surfactant concentration in solution was 3.0 mM and the final salicylate concentration ~ 2 mM.) The hexagonally packed spherical aggregates transform to parallel flexible cylinders, indicating an increase in g due to partial neutralization of the headgroup by specific binding of salicylate. The shape transformation was visible within ~ 2 min of adding salicylate, which was the time required to equilibrate the salicylate concentration throughout the fluid cell.

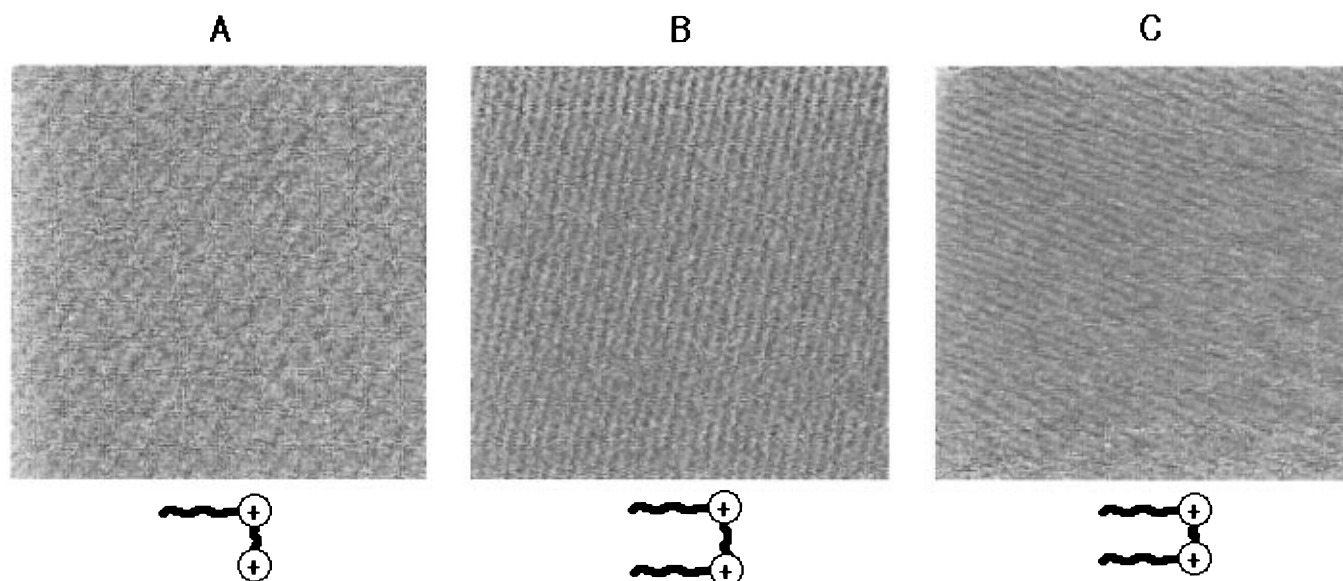


Figure 3. AFM images (150×150 nm) of gemini surfactant aggregates on the cleavage plane of graphite. All images show stripes oriented *perpendicular* to an underlying graphite symmetry direction (determined by lattice resolution scans, not shown), consistent with half-cylindrical aggregates with the bottom plane of tailgroups parallel to a graphite symmetry axis.^{1,2} (A) Asymmetric gemini surfactant C_{18-3-1} (3.0 mM solution), showing an interaggregate spacing of 6.3 ± 0.6 nm. C_{16-3-1} showed similar aggregates with a measured spacing of 6.1 nm. (B) Symmetric gemini surfactant $C_{12-4-12}$ (2.2 mM solution), showing an interaggregate spacing of 4.6 ± 0.5 nm. Similar images were obtained for $C_{12-6-12}$. (C) Symmetric gemini surfactant $C_{12-2-12}$ (1.0 mM solution), showing an interaggregate spacing of 4.0 ± 0.4 nm.

values which in any case favor cylindrical curvature, they are rather unexpected for asymmetric geminis having low g , which should form cylinders only reluctantly. A study¹⁷ of C_{12-3-1} (with Cl^- counterions) has shown that the solution phase behavior is dominated by a micellar cubic phase, with a cylindrical hexagonal phase expressed only at high concentrations relative to conventional surfactants; in our experiments on mica, even 1 M solutions of C_{16-3-1} still showed only spherical micelles at the interface (not shown). The ability of graphite to template half-cylindrical structures of C_{n-3-1} is therefore an indication that surface-tailgroup interactions are stronger than interactions between neighboring tailgroups, as evidenced also by calorimetry studies on conventional surfactants.³³

This surface control may have interesting consequences for surfactant-based templating. Thin films of surfactant-silicate mesophases nucleated at mica-solution inter-

faces^{8,10} have always shown the same architecture as mesophases nucleated in solution, with the influence of the mica limited to orientation of the mesophase. This can now be understood with reference to Table 1 (columns 2 and 3); since the mica surface and silicate anions have similar effects on cationic micelles, there is no conflict between preferred morphologies. For nucleation on graphite, however, a conflict often exists between the curvature favored by the surfactant-silicate mesophase and that favored by the surface (columns 2 and 4 of Table 1). In particular, the mesophase formed by C_{18-3-1} and silicates is known to have a spherical hexagonal morphology when precipitated from solution,⁷ which is at odds with the half-cylindrical self-assembly favored by C_{18-3-1} at the graphite-solution interface. To determine which effect is dominant in this case, an interfacial C_{18-3-1} -silicate mesophase was nucleated on graphite by covering

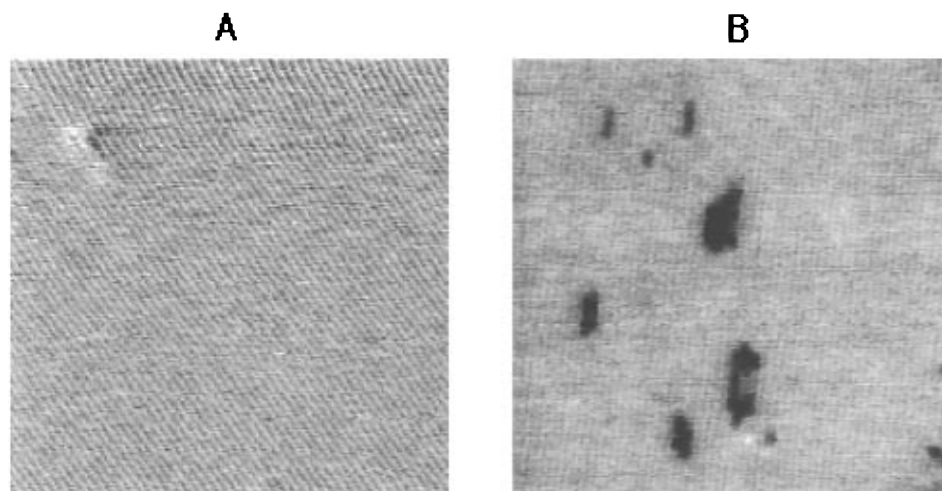


Figure 4. AFM images (350×350 nm) of C_{18-3-1} -silicate interfacial structures at a graphite surface. (A) A “wet mesophase” formed from acidic conditions by covering the graphite surface in precursor solution (0.007 g of tetraethyl orthosilicate (TEOS) and 0.018 g of C_{18-3-1} in 1 mL of 0.5 M HCl) for ~ 2 h and rinsing in pure water without drying. (B) A dried interfacial film formed from basic conditions by covering the graphite surface in precursor solution (0.020 g of tetraethyl orthosilicate and 0.010 g of C_{18-3-1} in 1 mL of 0.2 M NaOH) and drying in an oven (~ 80 °C) for a few days; dark patches are defects in the linear surface pattern, revealing bare graphite underneath. (Though much of the resulting surface was covered with precipitate, the linear surface pattern could be clearly imaged on bare-looking patches of the sample surface.) In both cases the silicified layer reproduces the interfacial surfactant phase (cf. Figure 3A), in spite of the preferred morphology in solution being a micellar cage structure.⁷

a freshly cleaved surface with precursor solution in a 100% relative humidity environment (to prevent drying) for ~ 2 h. The surface was then gently rinsed without drying by exchanging thoroughly with pure water in the AFM fluid cell. Imaging in this water (Figure 4A) showed that an interfacial surfactant–silicate mesophase was left behind, clearly reproducing the linear (half-cylindrical) morphology favored by the graphite surface. A similar, though more defective, pattern could also be observed for a dried interfacial layer imaged in air (Figure 4B). (Such linear structures were not observed when mesophases of the same surfactants and silicates were nucleated on mica.³⁵) However, we emphasize that how far normal to the surface this pattern persists is still an open question; since a “spherical hexagonal” morphology is favored in bulk solution,⁷ the cylindrical curvature may be limited to just the interface. (Ordering normal to the film plane may be enhanced by acidic synthesis conditions.³⁵)

Conclusions

The central conclusion of this work is that the interaction area between a surfactant molecule and a surface determines the degree of control the surface exerts over the interfacial aggregate morphology. The graphite surface, for which the interaction area is highly asymmetric and covers virtually the entire axial area of the surfactant tailgroup, gives rise to interfacial aggregates that are predominantly half-cylindrical regardless of surfactant geometry. Silicification of these aggregates can result in an interfacial mesophase that differs from the structure favored in free solution. The mica surface, for which the interaction area is the much smaller and more symmetric headgroup area, gives rise to interfacial structures wherein surfactant geometry still plays an important role. Interfacial aggregates on mica follow the same general trend

of curvature vs packing parameter as do free aggregates, although with slightly different transitional values for g . Shape transitions of interfacial aggregates can be induced by specifically binding counterions. The close match observed between two-dimensional aggregate morphologies on mica and three-dimensional mesophases of surfactant–silicate nanocomposites confirms the central role of electrostatic interactions and provides a method for predicting and designing specific mesoscopic architectures.

If the relationship between interaction area and surface control of the aggregate phase proves widely applicable, dimeric and oligomeric surfactants³⁶ may have an important future role in the synthesis of mesoscopic interfacial films. Gemini aggregates on mica seem to show a closer registry with the mica lattice than do conventional surfactants, perhaps because the presence of *two* binding sites gives the geminis a larger interaction area with the mica lattice. Surface registry could be further enhanced by using surfactants with three or more binding sites,³⁶ or by tailoring the spacer to achieve an epitaxial match between the intercharge spacing and an existing periodicity on the mica lattice.

Acknowledgment. We thank M. Trau, E. Luther, G. G. Warr, S. M. Gruner, and K. M. McGrath for useful discussions and Digital Instruments for technical support. This work was supported by the U.S. Army Research Office (Grant DAAH04-95-1-0102) and the MRSEC program of the National Science Foundation (Award DMR-940032) (S.M. and I.A.A.), by NSF Grants DMR 95-20971 and MCB 92-02775 (G.D.S. and Q.H.), by the Office of Naval Research (S.M., P.K.H., D.E.M., and G.D.S.), and by a University of California Biotechnology Research and Education Training Grant (T.E.S.).

LA970070S

(35) Tolbert, S. H.; Schäffer, T. E.; Feng, J.; Hansma, P. K.; Stucky, G. D. *Chem. Mater.*, in press.

(36) Danino, D.; Talmon, Y.; Levy, H.; Beinert, G.; Zana, R. *Science* **1995**, *269*, 1420–1421.

(37) Warr, G. G.; Sen, R.; Evans, D. F.; Trend, J. E. *J. Phys. Chem.* **1988**, *92*, 774–783.